Proceedings in Manufacturing Systems, Volume 19, Issue 4, 2024, pp. 143-150 ISSN 2067-9238

DESIGN AND STRUCTURAL ANALYSIS OF A ROBOTIC PLATFORM FOR LOGISTIC SYSTEMS

Constantin-Adrian POPESCU[1*], Tudor George ALEXANDRU[2], Emilia-Maria POPESCU[3], Cicerone Laurențiu POPA[4], Cristina-Luciana DUDICI[5]

[1,2,3,5)] Lecturer, PhD, Robots and Manufacturing Systems Dep., National University of Science and Technology POLITEHNICA Bucharest
[4)] Assoc. Prof., PhD, Robots and Manufacturing Systems Dep., National University of Science and Technology POLITEHNICA Bucharest

Abstract: *In the present industrial context, logistic robotic platforms play a crucial role in automating material handling, improving efficiency, and reducing operational costs in warehouses and manufacturing environments. This study presents numerical simulation and analytical methodologies for evaluating the structural integrity of such solutions. A simplified model was developed, retaining only the essential structural components, which were interconnected using constraint equation rigid elements. Secondary elements were suppressed and accounted for through 0D mass elements, incorporating known mass and moment of inertia properties. The analysis considered the worst-case scenario, involving maximum acceleration and payload, combined with swivel plate indexing. Additionally, the reactions induced by the belt drive were calculated and integrated as defined loads. Finite element analysis was conducted using ANSYS APDL, with fringe plots generated for the displacement vector sum. Nodal extractions were performed to assess the tension and shear loads at critical assembly junctions. Furthermore, L-type metal structure and bolted assembly evaluation was completed. All analytical methodologies were implemented in Fortran95 language. The findings provide insights into the platform's load-bearing capacity and stress distribution, ensuring its structural integrity. The results achieved were subsequently employed in the physical prototyping of the assembly, validating the proposed design and analysis methodologies.*

Key words: *Logistics, Robotics, Simulation, APDL, Fortran95.*

1. INTRODUCTION

Robotic systems are essential in modern industrial environments due to their ability to enhance efficiency, flexibility, and adaptability across a wide range of applications. These solutions are no longer limited to fixed positions. Instead, they can navigate through complex environments with ease, making them especially valuable in manufacturing systems. For instance, mobile units capable of off-road operation and carrying independent energy sources demonstrate a high degree of versatility [1].

Recent advancements have further expanded their functionality, with the integration of vision systems and robust control strategies enabling operation in unstructured environments. These enhancements extend operational lifespans while simultaneously reducing maintenance and labor costs [2]. Additionally, cloud collaboration architectures now support predictive maintenance and real-time supervisory control, critical capabilities for scalable industrial automation [3]. Open and modular designs, such as those found in platforms like VEGO, not only improve adaptability but also facilitate engineering education and skills development [4].

At the core of such innovation lies the importance of structural analysis during the design phase. Ensuring mechanical integrity is vital for both performance and safety under demanding operating conditions. Numerous studies have highlighted the value of finite element analysis (FEA) for identifying stress concentrations, optimizing structural weight relative to payload, and validating design scenarios prior to physical prototyping [5]. Simulation tools such as SolidWorks and ANSYS allow engineers to refine designs, improve mobility, and reduce strain on actuators by selecting optimal materials and structural layouts [6]. Moreover, accurate modeling contributes to system-level fault diagnosis by clarifying variable dependencies and improving error detection and localization in complex architectures [7].

This paper presents the design and structural analysis of a modular robotic platform tailored for logistics applications. The structure includes L-shaped steel framing for supporting dynamic loads. A hybrid drive system with Mecanum and rubber wheels powered by DC servo motors enables omnidirectional mobility. A belt-driven swivel plate mechanism provides rotational alignment. An electromagnetic coupling facilitates torque transfer with optional disengagement.

Verification of the structural integrity is carried out during the design stage through FEA conducted in ANSYS APDL. The simulation model comprises a simplified representation of the robotic platform's

[*] Corresponding author: Splaiul Independenței 313, district 6, 060042, Bucharest, Romania,
Tel. 0040 21 402 9420,
E-mail addresses: *popescuadrian_c@yahoo.com* (A. Popescu).

primary structure, where thick shell and beam elements are employed to model the load-bearing components. Structural connections are represented using constraint equations. Symmetry is included to enhance computational efficiency, limiting the analysis to a quarter of the total assembly. The inertial effects of secondary components are included through 0D mass elements by assigning appropriate mass and moment of inertia values. Belt drive reactions are derived analytically to capture the localized loading on the bearing mounts and swivel plate. The loads and Boundary Conditions (BCs), resulting from belt pretension and torque transmission between the drive and driven pulleys, are computed externally using dedicated routines developed in Fortran95. The simulation focuses on the worst-case operational scenario, accounting for maximum payload and acceleration, combined with indexing motion of the swivel plate. Post-processing of the FEA results includes nodal force extractions in critical junction areas, which are then used for analytical verification of bolted connections under combined tension and shear. These calculations, along with the margin of safety evaluation for the L-shaped steel framing, are also completed in Fortran95.

The remainder of this paper is organized as follows: Section 2 presents a schematic representation of the proposed structural evaluation methodology. Section 3 provides a detailed explanation of each constitutive module, including the initial CAD assembly, the simplified FEM simulation model, load case formulation and the underlying analytical methodologies. Section 4 outlines the results of the finite element simulations and analytical evaluations, with emphasize on displacement behavior, and validation of critical load-bearing junctions. Finally, Section 5 concludes the paper by summarizing the key findings and discussing their implications for the physical prototyping and structural robustness of the proposed design.

2. RELATED WORK

Computer-Aided Engineering (CAE) approaches related to the present work are depicted in [8]. The paper proposes a design, simulation, and optimization approach applicable to industrial robots, focusing on improving structural performance. The study combines FEA, kinematic simulation, and optimization algorithms to enhance the design workflow of robotic systems. It uses a simplified 3D model inspired by a KUKA-type six-axis robot for simulation and analysis.

FEA of robotic platforms is completed in [9]. The work emphasizes how CAE tools are employed in the design and verification phases of a six-degree-of-freedom (DOF) dual-arm robot developed for automated cabin docking. The robot's structure, including its left and right robotic arms, base, and joints, was modeled in NX 2023 software, a CAD and CAE-integrated platform. FEA was carried out by employing Simcenter Nastran to evaluate static stress, displacement, and strain for key load-bearing components. Structural simulation results were validated against the design specifications through physical prototype testing.

The work depicted in [10] outlines the development of an ROV-type underwater robot platform equipped with a 7-function electric manipulator to support autonomous underwater intervention tasks. The structural design had to accommodate a relatively large manipulator within a compact, lightweight frame suitable for water tank testing. Static and modal analysis was completed in ABAQUS for evaluating the critical stress and the mode shape results. Only the primary structure was included. The onboard components (manipulator, sensors, buoyancy blocks) were represented as concentrated point masses.

Other simulation approaches include the coupling between FEA and numeric computer environments. For example, the work depicted in [11] aims to analyze and optimize the structural and force characteristics of a 6-DOF Stewart-Gough type parallel robotic platform during movement along various trajectories. MSC Adams was used to build the digital model and perform multi-body dynamic simulations. Matlab Simulink provided the control and trajectory input environment. A Python–Adams interface enabled automated parametric model updates and batch simulations.

3. METHODOLOGICAL FRAMEWORK AND WORKFLOW

3.1. Schematic representation

The proposed approach consists of two layers of abstraction: the FEM simulation and the Fortran programming layer (Fig. 1). Each layer performs distinct but complementary tasks. The FEM Simulation Layer focuses on numerical modeling and virtual testing of the platform. In the first stage, a detailed CAD model of the robotic platform (§3.2) is developed. The geometry is subjected to simplification stages to create a computationally efficient FEM simulation model (§3.3). This model retains only the critical structural elements. Loads and boundary conditions (§3.4), including those derived from operational scenarios and belt drive reactions, are applied to simulate the most demanding working conditions.

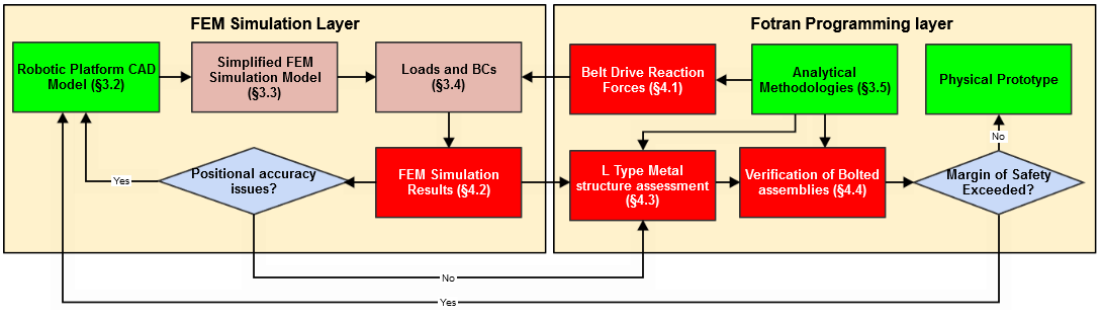

Fig. 1. The schematic representation of the proposed approach.

The simulation results (§4.2), are evaluated to determine the impact of the displacement vector sum on the positional accuracy of the robotic platform. If the requirements are not met, the process loops back to refine the CAD model. If the requirements are satisfied, the nodal extractions are feed into the analytical layer for further validation of the studied junctions.

The Fortran Programming Layer performs analytical calculations that complement the FEM results. It starts with the implementation of analytical methodologies (§3.5) using the Fortran95 language. These include the calculation of belt drive reaction forces (§4.1), which are then fed back into the FEM model to ensure that the loading conditions are fully considered. Key components such as the L-type metal structural elements (§4.3) and bolted assemblies (§4.4) are assessed under worst-case conditions using analytical techniques.

The margin of safety check is carried out to validate whether the structure can be safely prototyped. If the safety criteria are met, the workflow proceeds to the development of the physical prototype. If not, necessary revisions are made to the initial configuration.

3.2. The robotic platform CAD model

The illustrated assembly represents a logistic robotic platform engineered for flexible and efficient movement within industrial environments (Fig. 2). Its architecture integrates both mechanical and electromechanical subsystems, each tailored to support specific mobility and structural performance requirements. Central to the design is the structural framing, which provides the foundational support for the platform, housing all other subsystems. The platform features a hybrid mobility solution combining Mecanum wheels and standard rubber wheels. The Mecanum wheels are positioned at the corners, enabling omni-directional movement, allowing the platform to move forward, sideways, or diagonally without reorienting. This capability is critical for navigating in tight or cluttered environments. In contrast, the centrally mounted standard rubber wheels contribute to load-bearing and stability during linear motion, particularly when the swivel mechanism is engaged, disabling Mecanum functionality. Each Mecanum wheel is independently powered by an individual DC servo drive. A key feature in this system is the electromagnetic coupling, which allows selective engagement or disengagement of specific drive components, enabling mode switching between standard and omni-directional motion as needed.

The system's adaptability is further enhanced by a swivel plate, actuated by a gearbox stepper motor. This motor, paired with a reduction gearbox, provides the torque necessary to rotate sections of the platform. The swivel plate enables dynamic reorientation of the wheel assemblies, a crucial function for shifting between navigation modes or aligning the platform with docking stations or workstations.

3.3. The simplified FEM simulation model

The FEM simulation model illustrated in Fig. 3 represents a reduced-order representation of the robotic platform, developed by employing ANSYS R19.0. This modeling strategy can accurately capture the behavior of the main structural elements while reducing the

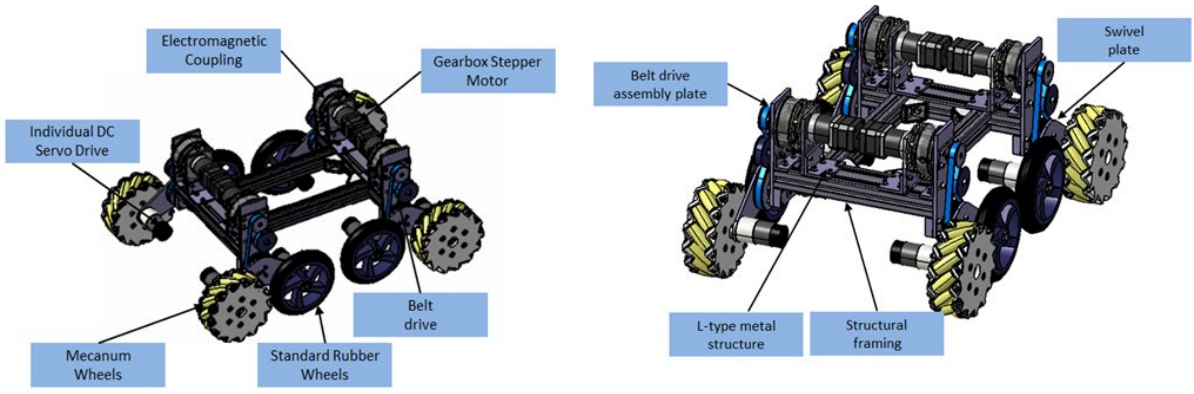

Fig. 2. Components of the studied assembly.

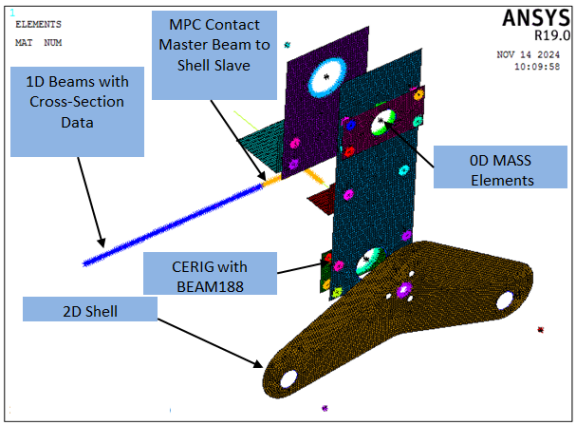

Fig. 3. Representation of the FEM Simulation model.

computational demands compared to a fully meshed 3D solid model. A selective combination of lower-dimensional element types such as 1D, 2D, and 0D is employed.

1D beam elements, defined with cross-sectional properties, are used to model the long, slender members frame components. These elements, implemented with BEAM188, can capture bending, axial, and torsional responses with minimal degrees of freedom compared to 3D solids. This substitution alone results in significant reductions in both element count and solution time, particularly for load-bearing members where cross-sectional behavior is more relevant than volumetric detail.

2D shell elements are employed for components like brackets and plates that primarily experience in-plane and bending stresses. By modeling these parts with shell elements instead of 3D solids, the model reduces the number of nodes and integration points required, further decreasing memory and processing demands. Despite this simplification, shell elements accurately represent the mechanical behavior of thin-walled parts, making them ideal for structural surfaces.

0D MASS elements are strategically placed to represent the inertial effects of omitted components such as the driving systems and the electromagnetic couplings. These elements carry no geometric representation but allow the inclusion of mass and moment of inertia.

To ensure connectivity and proper interaction between elements of different types, CERIG constraints are used for rigid coupling, and MPCs contact definitions establish interactions between beam and shell elements. These methods allow force and displacement transfer without requiring detailed contact meshes, which are usually computationally expensive.

In summary, the deliberate use of reduced-dimension elements such as 1D beams, 2D shells, and 0D masses help achieve a balance between computational efficiency and structural accuracy. This approach makes it highly suitable for iterative design loops, parametric studies or validation loops, where full 3D solid modeling would be time-consuming and resource-intensive.

3.4. Loads and BCs

The operational demands of the robotic platform under worst-case scenarios, including maximum payload, acceleration, and rotational velocity are taken into account. By combining the effect of the inertial loads, the applied forces and the realistic support conditions, the simulation ensures a high-fidelity assessment of the structural performance.

Standard Earth gravity acts on the entire structure, simulating the gravitational force. In addition, a linear acceleration vector is imposed to mimic the platform's movement during high-speed operation, generating realistic inertial reactions based on the mass of the entire assembly. For rotating components such as the swivel mechanism, a rotational velocity input introduces centrifugal effects, which are critical for parts subjected to angular motion.

0D mass elements are introduced to account for the mass and inertia of suppressed non-structural components. These include representations of the

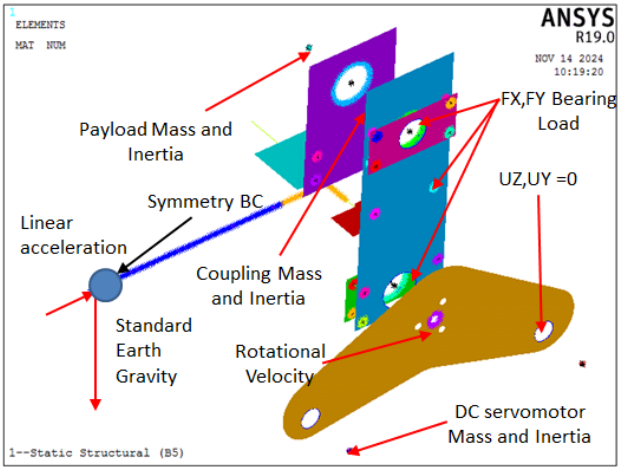

Fig. 4. Definition of the Loads and BCs.

payload, DC servomotor, and electromagnetic coupling. Each of these elements carries assigned mass and moment of inertia values, allowing the simulation to reflect realistic weight distribution and dynamic influence without the computational cost of modeling detailed 3D geometries.

The model also incorporates mechanical loading conditions, notably bearing loads in the FX and FY directions. These are applied in the locations where the assembly interfaces with supporting or rotating elements, such as shafts or swivel joints. These loads simulate reaction forces that arise from the constraints imposed by real mechanical bearings or contact points during motion.

A set of boundary conditions restrain the motion of the assembly relative to the ground. A symmetry boundary condition is defined based on two symmetry planes for reducing the model's size and complexity while preserving its mechanical behavior.

Figure 4 illustrates the applied constraints.

3.5. Analytical methodologies

The FEM simulation model results include the nodal reactions, essential for the analytical verification of the L Type metal structures and the bolted assemblies.

L-type metal structure assessment. The methodology for sizing L-type metal structure is derived from ANSI/AISC 360-22 Specification for Structural Steel Buildings [12]. When an L-bracket is loaded in tension on one leg, while clamped on the other the load is transferred through bolts. Thus, the net section is critical:

$$A_{net} = (w - d_h - 2c) \cdot t, \tag{1}$$

where: w – width of the leg under tension, d_h – diameter of the hole, c – edge clearance and t – thickness.

The primary stress is the axial stress, defined as the applied tensile load acting on the net section:

$$\sigma = P / A_{net}. \tag{2}$$

Failure can occur due to the gross section yielding:

$$\sigma_g = P / A_{gros} \leq \sigma_y, \tag{3}$$

where A_{gross} represents the total cross sectional area of the loaded leg, calculated as:

$$A_{gros} = w \cdot t. \quad (4)$$

The net section fracture can be evaluated by comparing the primary stress with the tensile yield strength.

In the location of the bolted junction, bearing failure can occur:

$$\sigma_b = P / (t \cdot d_h) \leq \sigma_{bearing}, \quad (5)$$

where: $\sigma_{bearing}$ represents the bearing allowable.

Tearout of the bolt holes can be calculated based on:

$$F_{tearout} = 2 \cdot t \cdot c \cdot \tau_{allowable}. \quad (6)$$

Verification of bolted assemblies. The verification of the fasteners is completed as per ISO 898-1 [13]. For metric bolts, the tensile stress area As is defined as:

$$A_s = \pi/4 \cdot (d - 0.9382 \cdot P)^2, \quad (7)$$

where: d – nominal diameter and P – thread pitch.

The shank area can be calculated as:

$$A_b = \pi/4 \cdot d^2. \quad (8)$$

The material yield and ultimate strength is determined based on the bolt property class (i.e. 8.8 or 10.9).

To calculate the tension allowable:

$$F_t = (f_u \cdot A_s) / SF, \quad (9)$$

where: f_u – ultimate tensile strength of the bolt, A_s – tensile stress area and SF – safety factor.

The shear allowable is typically taken as a percentage of the ultimate tensile strength:

$$f_{shear} = k \cdot f_u, \quad (10)$$

where k – coefficient as an engineering approximation ($k = 0.6$). Then:

$$F_{s,\,allow} = (f_{shear} \cdot A_b) / SF. \quad (11)$$

The loads required for completing the analytical calculations of the L-type brackets and bolted junctions are derived from the nodal reactions of the FEM simulation model.

Planar belt drive system reaction forces. The purpose of the methodology is to estimate the bearing loads on pulleys in a planar belt drive system subject to torque and pretension, using classical mechanics and belt friction theory [14, 15]. Figure 5 illustrates the studied configuration.

The driving pulley transmits torque Tq through the difference in belt tensions:

$$T_q = (T_1 - T_2) \cdot r_1. \quad (12)$$

where: T_1 and T_2 – tight and slack-side tensions and r_1 – radius of the driving pulley.

Assuming no slip, the Euler-Eytelwein equation describes belt tensions:

$$T_1 / T_2 = e^{\mu\alpha}, \quad (13)$$

where: μ – coefficient of friction and α – wrap angle.

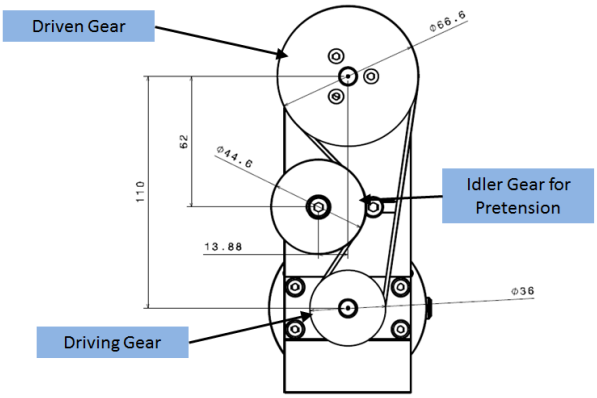

Fig. 5. The studied configuration of the belt drive system.

If an idler applies a uniform pretension T_{pret}, both tensions are offset equally:

$$T'_1 = T_1 + T_{pret},$$
$$T'_2 = T_2 + T_{pret}. \quad (14)$$

The direction of each belt force is given by the unit vector between pulley centers:

$$\hat{u}_{ij} = \frac{1}{\sqrt{(x_j - x_i)^2 + (y_j - y_i)^2}} \begin{pmatrix} x_j - x_i \\ y_j - y_i \end{pmatrix}. \quad (15)$$

Each pulley bears the vector sum of tensions from the incoming belt segments (F_1, F_2 and F_3).

$$F_1 = T'_1 \hat{u}_{13} + T'_2 \hat{u}_{12}$$
$$F_2 = T'_1 \hat{u}_{31} + T'_2 \hat{u}_{32}. \quad (16)$$
$$F_3 = T'_1 \hat{u}_{23} + T'_2 \hat{u}_{21}$$

The calculated bearing loads are defined as input in the FEM simulation model.

Implementation of the Fortran95 procedures. This procedure starts by reading design inputs such as torque, pulley radii, friction, and wrap angles:

```
real :: Tq, r1, mu, alpha, T1, T2, Tpret
read(*,*) Tq, r1, mu, alpha, Tpret
```

Euler-Eytelwein equation are employed for more accurate modeling:

```
T2 = Tpret
T1 = T2 * exp(mu * alpha)
```

Resolving belt forces into components:

```
real :: Fx, Fy, angle
angle = atan2(y2 - y1, x2 - x1)
Fx = T1 * cos(angle) + T2 * cos(angle +
pi)
Fy = T1 * sin(angle) + T2 * sin(angle +
pi)
```

Output for integration with FEM:

```
open(unit=15, file='belt_forces.dat')
write(15,'(2F12.5)') Fx, Fy
close(15)
```

These values are then used in ANSYS to define *FX* and *FY* boundary loads for bearing points.

In ANSYS APDL, nodal forces are needed for external analytical processing are extracted using commands such as:

```
*GET, fx, NODE, 101, RF, X
! Get force in X direction at node 101
*VWRITE, fx
(F12.5)
! Write force to file
```

These results are saved into a formatted text file that is read line-by-line in the Fortran95 routines using standard file I/O operations.

This methodology verifies if a bracket under tensile loading meets structural integrity criteria. The process begins by reading input forces and dimensions:

```
real :: P, w, dh, c, t, Anet, Agross,
sigma, sigma_g, sigma_b
open(unit=10,      file='nodal_forces.dat',
status='old')
read(10,*) P
close(10)
```

Afterwards, the net area and gross area are calculated by employing:

```
Anet = (w - dh - c) * t
Agross = w * t
```

Then the stresses are calculated:

```
sigma = P / Anet
sigma_g = P / Agross
sigma_b = P / (dh * t)
```

Finally, conditional checks verify compliance:

```
if (sigma < yield_strength .and. sigma_b <
bearing_limit) then
    print *, 'Bracket PASSES all stress
checks.'
else
    print *, 'Bracket FAILS - Redesign
required.'
endif
```

The bolt verification routine begins by loading force data and bolt specs:

```
real :: Ftens, Fshear, d, P, As, fu, SF,
F_allow_tens, F_allow_shear
open(unit=11,      file='bolt_forces.dat',
status='old')
read(11,*) Ftens, Fshear
close(11)

As = 0.7854 * (d - 0.9382 * P)**2     !
Tensile stress area for metric bolt
```

Tensile and shear allowables:

```
F_allow_tens = As * fu / SF
F_allow_shear = As * 0.6 * fu / SF
```

Verification condition:

```
if (Ftens <= F_allow_tens .and. Fshear <=
F_allow_shear) then
    print *, 'Bolt PASSES verification.'
else
    print *, 'Bolt FAILS - Recalculate or
increase grade.'
endif
```

Log writing for traceability:

```
open(unit=20,      file='bolt_report.txt',
status='unknown')
write(20,*) 'Bolt Check:', Ftens, Fshear,
F_allow_tens, F_allow_shear
close(20)
```

4. RESULTS AND DISCUSSION

This section summarizes the results of the FEM simulation and analytical calculations.

4.1. Planar belt drive system reaction forces

The reaction forces of the belt drive system are depicted in Table 1.

4.2. FEM Simulation results

Figure 6 depicts the fringe plot for the displacement vector sum.

The maximum deflection occurs at the level of the swivel plate bearing unit, having a value of 36 μm in the radial direction. This result can be explained by the belt pretension loads. In the location where the wheel assembly is mounted the maximum deflection has a low order of magnitude (less than 8 μm). On the other hand, the structural framing maintains the desired stiffens, given the maximum deflection value of 4.3 μm.

Table 1

Summary of belt drive system reaction forces

Parameter	Value	
Input torque	0.524 Nm	
Driving pulley rotational velocity	0.582 RPM	
Diameter of the driving pulley	36 mm	
Diameter of the driven pulley	66 mm	
Diameter of the idler pulley	44 mm	
Coefficient of friction - μ	0.3	
Idler pulley pretension load	128 N	
Driving pulley net force	F_x	168.85 N
	F_y	195.13 N
Idler pulley net force	F_x	−247.2 N
	F_y	108.6 N
Driven pulley net force	F_x	78.44 N
	F_y	−303.79 N

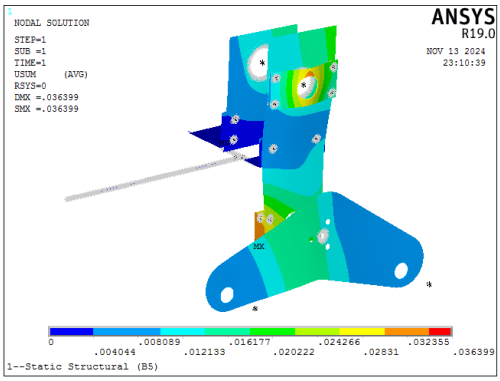

Fig. 6. Displacement vector sum fringe plot.

Thus, there is no impact on the positional accuracy of the entire assembly.

4.3. L-type metal structure assessment

The L-type metal structure that is subjected to the most severe tension load is located at the belt drive assembly plate and the structural framing junction (Fig. 7 – highlighted in yellow color). In this location, the highest forces generated from belt torque, pretension, and motion are transferred into the frame. The results are depicted in Table 2

The most severely loaded L-type aluminum structure is manufactured from 3003-H14 alloy. Key geometric and material parameters were used to evaluate stresses and failure modes. The applied load of 876.2 N resulted in a maximum net section stress of 18.25 MPa and gross section stress of 9.95 MPa, both within material yield limits.

Bearing stress (31.28 MPa) remained below the allowable bearing stress (193 MPa), and the tear-out capacity (1158 N) exceeded the applied load, ensuring structural integrity.

4.4 Verification of bolted assemblies

The fastener group that is subjected to the most severe tension and shear loads is also located at the belt drive assembly plate and the structural framing junction. M4 bolts of property class 8.8 ($f_u = 800$ MPa) were analyzed. Allowable tensile and shear loads per bolt were calculated as 4681.9 N and 4201.2 N, respectively. The FEM results revealed tensile and shear loads of 824 N and 306 N per bolt, yielding safety factors exceeding 2 (Table 3).

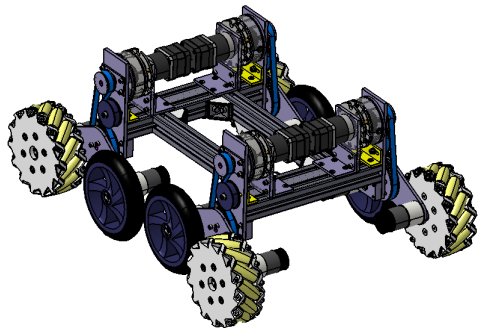

Fig. 7. Visualisation of the critical L-type brackets.

Table 2

Summary of the most critical L-type metal structure

Parameter	Value
w	22 mm
dh	7 mm
c	1.5*
t	4 mm
P	876.2 N
σ_y	152 MPa**
$\sigma_{bearing}$	193 MPa**
$\tau_{allowable}$	96.5 MPa**
A_{net}	48 mm^2
A_{gross}	88 mm^2
σ	18.25 MPa
σ_g	9.95 MPa $\leq \sigma_y$
σ_b	31.28 MPa $\leq \sigma_{bearing}$
$F_{tearout}$	1158 N

*c is considered 1.5 for conservatism

**Material properties as per Aluminum 3003-H14 [16]

7. CONCLUSIONS

The objective of this work was to design and validate the structural elements of a modular robotic platform intended for logistics applications.

The assembly was subjected to withstand worst-case operational conditions involving maximum acceleration, payload, and rotational motion conditions. This objective was achieved by combining finite element analysis and analytical calculations. The robotic assembly featured a structural frame built from L-shaped steel profiles. Its mobility system consisted of a hybrid configuration that included Mecanum wheels for omnidirectional motion and standard rubber wheels for linear travel. The solution also included a swivel mechanism and electromagnetic couplings to manage torque transmission and allow reconfiguration. The simulation model was developed using ANSYS APDL and employed a reduced-order modeling strategy. Primary structural elements were modeled using 1D beam and 2D shell elements, while 0D mass elements captured the inertial effects of omitted subsystems. Rigid coupling and constraint equations ensured proper interaction between these elements. Only a quarter of the full model was analyzed, significantly reducing computational demands without compromising accuracy. Analytical methodologies were used to supplement the simulation results and to compute key FEM input parameters. Belt drive reaction forces were derived using friction theory, implemented through Fortran95 routines. These forces were employed as input in the FEM model. Nodal forces were extracted and used to verify the structural adequacy of L-type brackets and bolted joints under combined loading conditions. The results indicated that the maximum displacement in the structure was 36 μm at the swivel bearing unit, which is within acceptable limits for maintaining positional accuracy. The L-type bracket subjected to the highest

Table 3

Safety factors of the most critical bolted joint

Parameter	Value
d	4 mm
P	0.7 mm
A_s	8.77 mm^2
A_b	12.56 mm^2
Property class	8.8
fu	800 MPa
SF	1.5
F_t	4681.9 N
k	0.6
$fshear$	480 MPa
Fs allowable	4201.2 N
FEM Tensile Load	824 N
FEM Shear Load	306 N
Safety Factor Tension	> 2
Safety Factor Shear	> 2

load exhibited stresses well below yield thresholds, and the tear-out capacity exceeded the applied forces. Similarly, the bolted joints maintained safety factors above two for both tensile and shear loading. The results validate the design approach, enabling the transition to physical prototyping. Nonetheless, the study has limitations. The FEM model was simplified and detailed geometry and dynamic behavior excluded. Fatigue effects, and thermal influences were not taken into account. Moreover, the analysis focused on a quasi-static loading scenario, which may not capture all real-world conditions. Future work should address these limitations by incorporating dynamic simulations, and fatigue analysis.

Funding: This research was funded by the National Program for Research of the National Association of Technical Universities – GNAC ARUT 2023, grant number 156/04.12.2023.

REFERENCES

[1] I.C. Ivan, M. Ghinea and G. Enciu, *SIMI RFID identification system in FMS logistics*, Annals of DAAAM & Proceedings, 2008, pp. 653-655.

[2] A. Andrei, A.F. Nicolescu and C. Pupăză, *Perspectives of virtual commissioning using ABB RobotStudio and Simatic robot integrator environments: a review,* Proceedings in Manufacturing Systems, Vol. 16, Iss. 3, pp. 117-123.

[3] D. Popescu, R. Iacob, R. Parpala and T. Dobrescu, *Virtual to real in robotic assembly/disassembly tasks*, UPB Sci. Bull., Series D, Vol. 78, Iss. 2, pp. 105-114.

[4] J.M. Lee, X. Xia, F. Chua, and Y. Guan, *VEGO: A novel design towards customizable and adjustable head-mounted display for VR. Virtual Reality & Intelligent Hardware*, Vol. 2, Iss. 5, pp. 443-453.

[5] G. Constantin, *Virtual Parametric Mechanical Design Associated with CAD Environment and Database*, Conference proceedings of eLearning and Software for Education (eLSE), Vol. 16, Iss. 03, 2020, pp. 192-202.

[6] J. Zhang, L. Wang and Jing, L., *Static Analysis of Manipulator Based on Solidworks and ANSYS Workbench,* Journal of Physics: Conference Series, Vol. 2477, Iss. 1, 2023, Article: 2477.

[7] M. Szvetits and U. Zdun, *Systematic literature review of the objectives, techniques, kinds, and architectures of models at runtime*, Software & Systems Modeling, Vol. 15, 2023, pp. 31-69.

[8] C. Pupăză, G. Constantin, Ș. Negrilă, *Computer aided engineering of industrial robots*, Proceedings in Manufacturing Systems, Vol. 9, Iss. 2, 2014, pp. 87-92.

[9] R. Liu and F. Pan, *Design and analysis of the mechanical structure of a robot system for cabin docking,* Actuators, Vol. 13, No. 6, 2024 Article: 206.

[10] T. K. Yeu, Y.J. Lee, Y.G. Lee and S.M. Yoon, *Preliminary study on identification of ROV for autonomous manipulation,* OCEANS 2019-Marseille, 2019, pp. 1-6.

[11] D. Sosa-Méndez, E. Lugo-González, M. Arias-Montiel, and R.A. Garcia-Garcia, *ADAMS-MATLAB co-simulation for kinematics, dynamics, and control of the Stewart–Gough platform*, International Journal of Advanced Robotic Systems, Vol. 14, Iss. 4, 2017, pp. 1-10.

[12] American Institute of Steel Construction, Specification for Structural Steel Buildings (ANSI/AISC 360-22), available at: `https://www.aisc.org/Specification-for-Structural-Steel-Buildings-ANSIAISC-360-22-Download`, accessed: 2025-07-09.

[13] Internation Standard Organization, Mechanical properties of fasteners made of carbon steel and alloy steel (ISO 898-1), available at: `https://cdn.standards.iteh.ai/samples/60610/e211f7b6697643f192d041ceceb1f2be/ISO-898-1-2013.pdf`, accessed: 2025-07-09.

[14] V. Zamfir, N. Nitescu and G. Dimirache, *Organe de masini. Transmisii prin curele. Transmisii prin lanturi*, Litografia Universității din Petroșani, Petroșani, 1992.

[15] J.E. Shigley, C.R. Mischke and R.G. Budynas, *Mechanical Engineering Design (10th ed.)*, McGraw-Hill, New York, 2015.

[16] MATWEB LLC., Aluminum 3003-H14, available at: `https://www.matweb.com/search/datasheet.aspx?MatGUID=09c63ea8e10e4eea8398256801bb8514&ckck=1`, accessed: 2025-07-09.